Full-range stress-strain curves for aluminum alloys

Xiang Yun[a,b,c], Zhongxing Wang[d,e], Leroy Gardner[a]

[a] Department of Civil and Environmental Engineering, South Kensington Campus, Imperial College London, London SW7 2AZ, UK

[b] Department of Civil and Environmental Engineering, The Hong Kong Polytechnic University, Hong Kong

[c] Chinese National Engineering Research Centre for Steel Construction (Hong Kong Branch), The Hong Kong Polytechnic University, Hong Kong

[d] School of Civil Engineering, Key Laboratory of Coast Civil Structure Safety of China Ministry of Education, Tianjin University, Tianjin 300072, PR China

[e] Department of Civil Engineering, Tsinghua University, Beijing 10084, PR China

Abstract: Aluminum alloys are being increasingly used in a wide range of construction applications owing to their sound mechanical properties, lightness in weight, strong corrosion resistance, ability to be formed into complex and efficient cross-section shapes and natural aesthetics. Aluminum alloys are characterized by a rounded stress-strain response, with no sharply-defined yield point. Such behavior can be accurately represented using Ramberg-Osgood-type equations. In the present study, use of a two-stage Ramberg-Osgood model to describe the full-range stress-strain behavior of aluminum alloys is proposed and, following careful analysis of a comprehensive database of aluminum alloy coupon test data assembled from the literature, standardized values or predictive expressions for the required input parameters are derived. The experimental database includes over 700 engineering stress-strain curves obtained from 56 sources and covers five common aluminum alloy grades, namely 5052-H36，6061-T6, 6063-T5, 6082-T6 and 7A04-T6. The developed model is shown to be more accurate in predicting the full-range stress-strain response of aluminum alloys than existing expressions, and is suitable for use in the analytical modeling, numerical simulation and advanced design of aluminum alloy structures.

Keywords: Aluminum alloys, Constitutive modeling, Material modeling, Ramberg-Osgood

model, Stress-strain curves, Numerical modeling

Introduction

There are a wide variety of aluminum alloys with a broad range of mechanical properties. The different alloys are created through the addition of different levels of alloying elements, such as copper, magnesium, silicon and zinc, to the base aluminum metal. Depending on their chemical composition, aluminum alloys are grouped into seven series, the general characteristics of which have been discussed by Dwight (1998). The 5××× and 6××× series alloys, particularly grades 5052, 6061, 6063 and 6082, are well suited to applications in construction, with a good combination of strength, weldability, formability and corrosion resistance. Some 7××× series alloys (e.g. grade 7A04), offering higher strengths but reduced corrosion resistance and formability compared to the 6××× series alloys (Dwight 1998; CEN 2007) are also emerging in the structural field (Wang et al. 2020). The 6××× and 7××× series alloys are heat-treatable alloys that gain their strength by means of heat treatment, while the non-heat treatable 5××× series alloys can be enhanced in strength through cold-working during their manufacturing process.

The stress-strain behavior of aluminum alloys is characterized by a rounded response with no sharply defined yield point, which differs significantly from that of hot-rolled carbon steels (Yun and Gardner 2017). In addition, the stress-strain curves of aluminum alloys with different grades display differing degrees of nonlinearity, roundedness in the "knee" region (i.e. the region of the yield strength) and strain hardening, due primarily to their different chemical compositions and tempers.

With the increasing use of advanced analysis in the design of metallic structures (Gardner et al.

2019), it is imperative to improve current code provisions (Aluminum Association 2010; CEN 2007; Standards Australia 1997) and to develop an accurate and practical material model to describe the full-range stress-strain behavior of aluminum alloys; this is the focus of the present study.

For predicting the stress-strain characteristics of cold-formed steel and stainless steel, which exhibit a similar form of rounded response to aluminum alloys, the modified two-stage Ramberg-Osgood model has become the formulation of choice, providing both accuracy and practicality (Mirambell and Real 2000; Rasmussen 2003; Arrayago et al. 2015; Gardner and Yun 2018). An assessment of the applicability of the two-stage Ramberg-Osgood model to aluminum alloys and the derivation of standardized values or predictive equations for the key input parameters are presented herein. Focus is placed on five common structural aluminum alloys – 5052-H36, 6061-T6, 6063-T5, 6082-T6 and 7A04-T6. The developments are based on the analysis of an assembled experimental database comprising over 700 tensile stress-strain curves collected from 56 sources from around the world.

Existing stress-strain models

The engineering (nominal) stress-strain response of aluminum alloys is characterized by a continuous rounded curve with an absence of a sharply defined yield point, as shown in Fig. 1. More specifically, the curve features an initial linear-elastic region up to the proportional stress f_p, which is generally taken as the 0.01% proof stress, followed by a nonlinear "knee" region up to the conventionally defined yield strength f_y (i.e. the 0.2% proof stress) and strain hardening, the extent of which varies between grades, before reaching the ultimate tensile strength f_u and corresponding ultimate strain ε_u. The initial slope of the stress-strain curve and the tangent slope at the 0.2% proof stress are denoted E and $E_{0.2}$, respectively.

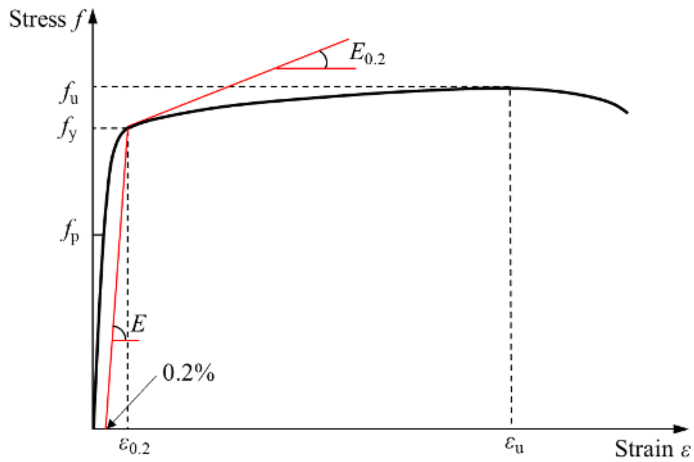

Fig. 1. Typical engineering (nominal) stress-strain curve for aluminum alloys

A number of material models have been developed to describe the nonlinear stress-strain behavior of aluminum alloys, with the simplest being piecewise linear models. The piecewise linear models defined in EN 1999-1-1 (CEN 2007) consist of two or three straight lines (corresponding to a bi-linear or a tri-linear material model, respectively) with each line representing a certain region of the stress-strain curve, with or without allowance for strain hardening, as shown in Fig. 2. In the piecewise linear models where strain hardening beyond the 0.2% proof stress is ignored − see Figs. 2(b) and 2(d), strains up to ε_u are allowed, while in cases where strain hardening is considered and represented by a sloped line − see Figs. 2(a) and 2(c), a cut-off strain equal to $0.5\varepsilon_u$ is defined to avoid over-predictions of strength in the strain hardening range. It can be seen from Fig. 2 that the piecewise linear models, particularly the idealized bi-linear model (Fig. 2(b)), fail to capture the roundedness of the stress-strain response that is characteristic of aluminum alloys. For sophisticated numerical simulations and advanced inelastic design methods (Fieber et al. 2020; Gardner et al. 2019; Walport et al. 2019), a more accurate and continuous full-range stress-strain model is required.

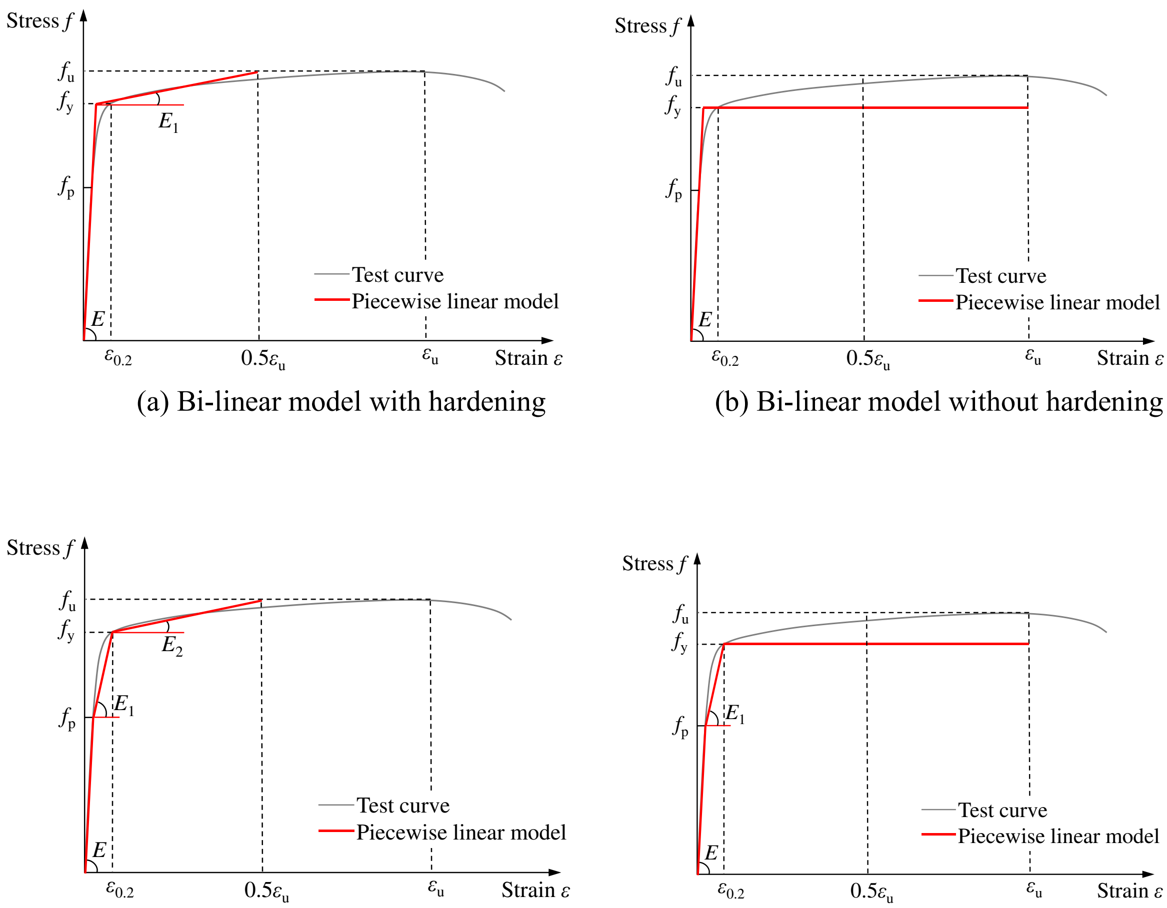

(a) Bi-linear model with hardening

(b) Bi-linear model without hardening

(c) Tri-linear model with hardening

(d) Tri-linear model without hardening

Fig. 2. Piecewise linear stress-strain models for aluminum alloys

Although other models exist (Baehre 1966; Mazzolani 1972, 1995), the most widely used continuous function to describe the rounded stress-strain behavior of metallic materials is the basic Ramberg-Osgood formulation (Ramberg and Osgood 1943), as modified by Hill (1944), or extensions thereof. The Ramberg-Osgood formulation, given by Eq. (1), has three basic input parameters − the Young's modulus E, the yield (0.2% proof) strength f_y and the strain hardening exponent n, and is adopted in the European standard EN 1999-1-1:2007 (CEN 2007).

$$\varepsilon = \frac{f}{E} + 0.002\left(\frac{f}{f_y}\right)^n \tag{1}$$

The determination of n requires, in addition to the conventional yield stress (i.e. 0.2% proof stress), the choice of a second reference point on the stress-strain curve. According to Annex E of EN 1999-1-1:2007 (CEN 2007), the second reference point may be taken as the 0.1% proof stress $\sigma_{0.1}$, located between f_p and f_y as illustrated in Fig. 3(a), for applications where only moderately small strains are expected to occur (e.g. in a buckling analysis); this results in Eq. (2) for the determination of the strain hardening exponent n.

$$n = \frac{\ln(2)}{\ln\left(f_y/\sigma_{0.1}\right)} \tag{2}$$

For analyses in which large strains are encountered (e.g. the simulation of manufacturing processes or connections), the strain hardening exponent n may be determined from Eq. (3), whereby the stress-strain curve passes through the point corresponding to the ultimate strength f_u, as shown in Fig. 3(b). In Eq. (3), $\varepsilon_{u,pl}$ is the plastic strain at f_u, which is equal to ($\varepsilon_u - f_u/E$); since the term f_u/E is relatively small in comparison to ε_u, $\varepsilon_{u,pl} \approx \varepsilon_u$.

$$n = \frac{\ln\left(0.002/\varepsilon_{u,pl}\right)}{\ln\left(f_y/f_u\right)} \approx \frac{\ln\left(0.002/\varepsilon_u\right)}{\ln\left(f_y/f_u\right)} \tag{3}$$

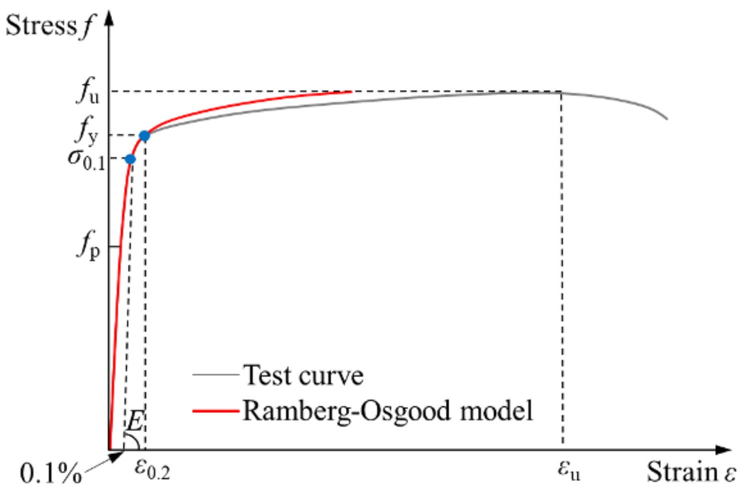

(a) Reference point corresponding to 0.1% proof stress $\sigma_{0.1}$

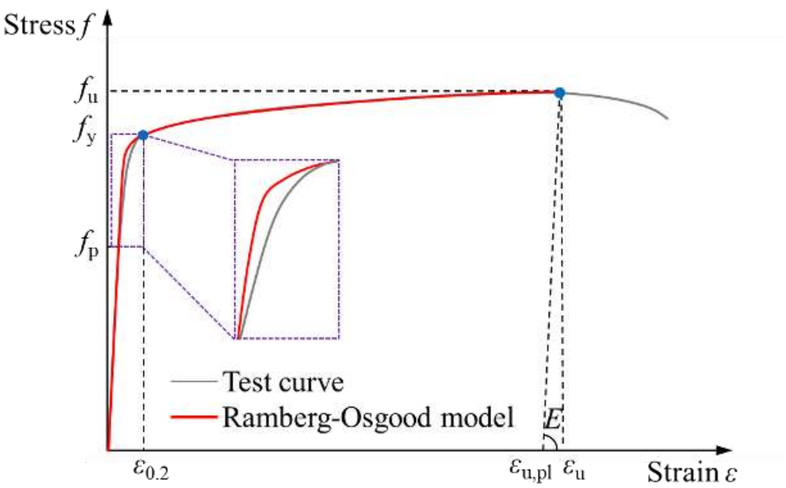

(b) Reference point corresponding to ultimate strength f_u

Fig. 3. Choice of reference point for determining strain hardening exponent n in Ramberg-Osgood model

While the Ramberg-Osgood formulation (Eq. (1)) provides an accurate representation of the degree of nonlinearity of certain regions of the stress-strain curve depending on the choice of the strain hardening exponent n, it does not, in general, provide an accurate representation of the full stress-strain curve, as highlighted in Fig. 3. This has led to the development of a number of two-stage Ramberg-Osgood models for stainless steels at room (Mirambell and Real 2000; Rasmussen 2003; Gardner and Ashraf 2006; Arrayago et al. 2015; Gardner 2019) and elevated temperatures (Gardner et al. 2010; Gardner et al. 2016) and cold-formed carbon steels (Gardner and Yun 2018). Three-stage models have also been proposed (Quach et al. 2008; Hradil et al. 2013).

The basic formulation of the two-stage Ramberg-Osgood models is given by Eq. (4), in which the nonlinear stress-strain curve is divided into two regions: below and above the yield (i.e. 0.2% proof) strength f_y. In Eq. (4), $E_{0.2}$ is the tangent modulus at the yield strength, illustrated in Fig. 1 and defined by Eq. (5), $\varepsilon_{0.2}$ is the total strain at the yield strength, equal to (f_y/E + 0.002), and m is the second strain hardening exponent, reflecting the degree of nonlinearity of the second region of the stress-strain curve (i.e. the region with strains ranging from $\varepsilon_{0.2}$ to ε_{u}). Note that a modified version of Eq. (4) was proposed by Rasmussen (2013), in which the term relating to the ultimate strain was simplified by setting $\left(\varepsilon_{u} - \left(\varepsilon_{0.2} + \frac{f_{u} - f_{y}}{E_{0.2}}\right)\right) = \varepsilon_{u}$; while this was appropriate for the studied (Rasmussen 2003) austenitic and duplex stainless steels, which have very high ductility (rendering $\varepsilon_{0.2}$ and $\left(f_{u} - f_{y}\right)/E_{0.2}$ small in comparison to ε_{u}), it is less suitable for less ductile materials, such as cold-formed steels (Gardner and Yun 2018) and ferritic stainless steels (Arrayago et al. 2015) studied previously and aluminum alloys studied herein. Hence, Eq. (4) is recommended for aluminum alloys and is used as the basis of the present study. Further information on the two-stage Ramberg-Osgood models proposed by different authors for stainless steels can be found in the review paper by Dundu (2018).

$$\varepsilon = \begin{cases} \dfrac{f}{E} + 0.002\left(\dfrac{f}{f_{y}}\right)^{n}, & \text{for } 0 < f \leq f_{y} \\ \dfrac{f - f_{y}}{E_{0.2}} + \left(\varepsilon_{u} - \varepsilon_{0.2} - \dfrac{f_{u} - f_{y}}{E_{0.2}}\right)\left(\dfrac{f - f_{y}}{f_{u} - f_{y}}\right)^{m} + \varepsilon_{0.2}, & \text{for } f_{y} < f \leq f_{u} \end{cases} \tag{4}$$

$$E_{0.2} = \frac{E}{1 + 0.002n\dfrac{E}{f_{y}}} \tag{5}$$

In the present paper, the full-range engineering stress-strain relationship for aluminum alloys is modeled using the two-stage Ramberg-Osgood model proposed by Mirambell and Real (2000) (see Eq. (4)). A comprehensive study is presented to determine values and predictive equations for the key input parameters, based on the analysis of a large database of experimentally obtained stress-strain curves on aluminum alloys collected from the literature and assembled in the following section.

Experimental database

In this section, engineering stress-strain curves obtained from tensile coupon tests on aluminum alloys are collected and analysed. A total of over 700 experimental stress-strain curves from 56 sources have been assembled, covering five grades that are commonly used in structural applications, namely 5052-H36, 6061-T6, 6063-T5, 6082-T6 and 7A04-T6, though the developed model is considered to be more broadly applicable. Note that the designation of aluminum alloys starts with a digit number that indicates the series to which the alloy belongs, and includes a letter after the hyphen that denotes the condition, or temper, of the alloy: "H" represents alloys whose strength is enhanced by cold-working while "T" signifies alloys that are thermally treated by different combinations of the following processes – solution annealing, tempering, quenching and artificial or natural ageing. More details about the designation system of aluminum alloys can be found in the American aluminum design manual (Aluminum Association 2010), the European standard EN 1999-1-1:2007 (CEN 2007) and Mazzolani (1995). With regards to the manufacturing method, extrusion is the most commonly used process to form aluminum alloy structural components, allowing complex cross-section geometries to be produced. Extrusion is especially suitable for aluminum alloys with good extrudability, e.g. the 6××× and 7××× series alloys; for the non-heat treatable 5××× series alloys, their high magnesium content limits their extrudability and hence cold-rolling is the principle production route (Huynh et al. 2019). Table 1 summarizes the key information relating to the assembled database of coupon test results, including the source, the material grade, the production method and cross-section profile of the members from which the coupons were extracted, the material thickness and the number of tests performed. It can be seen from Table 1 that the tested tensile coupons were extracted from a wide range of extruded or cold-rolled aluminum alloy profiles, including T-stubs, square, rectangular and circular hollow sections (SHS, RHS and CHS respectively), angle sections, plates, cruciform sections, channel sections, I-sections and irregular sections. Note that, although the coupon tests were conducted in accordance with different specifications, including AS (2007), CEN (2009) and ASTM (2013), the employed strain rates were all sufficiently low to be considered quasi-static (i.e. normally no higher than 0.00025 s^{-1}), and therefore to have little influence on the resulting stress-strain behavior (Huang and Young 2014). The mechanical properties of aluminum alloys at higher strain rates are out of the scope of the present study, but there remains scope for development of rate-dependent constitutive models for aluminum alloys considering the effect of high (dynamic) strain rates. It is also worthwhile to note that all stress-strain curves collected in the present study are from tensile coupon tests performed at room temperature. The deterioration of material properties of aluminum alloys 6063-T5 and 6061-T6 at elevated temperatures has been investigated by Su and Young (2019) while the effects of elevated temperatures on the material properties of other aluminum alloy grades need to be further investigated.

Table 1. Summary of key information relating to assembled database of aluminum alloy coupon tests

Source	Aluminum alloy grade	Production method	Thickness (mm)	Profiles of specimens from which coupons were extracted	Number of tests where E, f_y and f_u (ε_u) were provided[b]	Number of full stress-strain curves
Aalberg (2015)	6082-T6	Extrusion	4.6	I-sections	3 (0)	-
Alsanat et al. (2019)	5052-H36	Cold-rolling	2.5/3	Lipped channel sections	5 (5)	-
Brando et al. (2015)	6082-T6	Extrusion	3.5/5/6	I-section/plate	3 (3)	-
Chen et al. (2017)	6061-T6	Extrusion	-	CHS	3 (0)	-
Chen et al. (2018)	6061-T6	Extrusion	-	I-section	1 (0)	-
Chen et al. (2020)	6061-T6	Extrusion	2	Plate	1 (0)	-
Cho and Kim (2016)	6061-T6	Extrusion	3	Plates	3 (0)	-
Davies and Roberts (1999)	6082-T6	Extrusion	-	I-sections	11 (0)	-
De Matteis et al. (2000)	6061-T6/ 6082-T6	Extrusion	-	T-stubs	2 (2)	-
Đuričić et al. (2017)	6082-T6	Extrusion	2	CHS	4 (0)	-
Faella et al. (2000)	6060-T6/ 6082-T6	Extrusion	2-15.1	SHS/RHS	38 (0)	-
Feng et al. (2017)	6061-T6/ 6063-T5	Extrusion	2.5/3	SHS/RHS	2 (2)	2
Feng et al. (2018)	6061-T6/ 6063-T5	Extrusion	1/2/2.5/3	SHS/RHS	6 (6)	6
Feng et al. (2020)	6061-T6/ 6063-T5	Extrusion	7/7.5	CHS	2 (2)	2
Feng and Young (2015)	6061-T6	Extrusion	1.7/2/3/3.2/ 5	CHS	5 (0)	-

Guo (2006)	6061-T6	Extrusion	-	SHS/RHS/CHS/Angle sections /T-stubs	53 (36)	-
Guo et al. (2020)	6061-T6/ 6082-T6	Extrusion	4	Plates	9 (9)	-
He et al. (2019)	6061-T6	Extrusion	3/4	SHS	6 (0)	-
Hopperstad et al. (1999)	6082-T6	Extrusion	2.5	Cruciform sections	1 (0)	-
Huynh et al. (2019)	5052-H36	Cold-rolling	2.5/3	Channel-sections	218 (146)	146
Islam and Young (2012)	6061-T6	Extrusion	1.6/2.3/3/3.2/5	SHS/RHS	8 (0)	-
Jiang et al. (2018)	6061-T6	Extrusion	-	RHS	1 (0)	-
Jiang et al. (2020)	6061-T6	Extrusion	6/7/10	RHS/plate	3 (0)	-
Kim and Cho (2014)	6061-T6	Extrusion	2/3	Plates	6 (0)	-
Liu et al. (2015)	6063-T5	Extrusion	-	Irregular sections	2 (2)	2
Liu et al. (2019a)	6061-T6	Extrusion	8/10	I-sections/plates	6 (0)	-
Liu et al. (2019b)	6082-T6	Extrusion	-	Plate	1 (0)	-
Mazzolani et al. (2011)	6000 series[a]	Cutting from extruded hollow profiles	1.85-6.35	Channel-sections	16 (0)	-
Ma et al. (2020)	6061-T6	Extrusion	-	I-section	1 (0)	-
May and Menzemer (2005)	6061-T6	Extrusion	-	Tee/Channel/ Angle sections	3 (0)	-
Rønning et al. (2010)	6082-T6	Extrusion	3/4/4.4/5	Plates	8 (8)	-
Rouholamin et al. (2020)	5052-H36	Cold-rolling	2.5/3	Lipped channel sections	10 (0)	-
Shi et al. (2018)	6061-T6	Extrusion	8/12	I-sections/plates	3 (0)	-
Su et al. (2014)	6061-T6/ 6063-T5	Extrusion	2.81-10.45	SHS/RHS	15 (15)	15
Su et al. (2015)	6061-T6/ 6063-T5	Extrusion	2.85-10.42	SHS/RHS	15 (15)	15
Su and Young (2019)	6061-T6/ 6063-T5	Extrusion	4.5	RHS	2 (2)	2
Tajeuna et al. (2015)	6061-T6	Extrusion	3.2/6.4/9.5	Plates	18 (17)	-
Tryland et al. (1999)	6082-T6	Extrusion	3/5/8	Tee section/SHS	3 (3)	-
Wang et al. (2019)	6061-T6	Extrusion	8/10/12	T-stubs	9 (9)	9
Wang et al. (2016a)	7A04-T6	Extrusion	8	Angle sections	8 (8)	8
Wang et al. (2020)	7A04-T6	Extrusion	24	Angle sections	4 (4)	4
Wang et al. (2018a)	6061-T6	Extrusion	-	I-sections	9 (9)	9
Wang et al. (2018b)	6061-T6	Extrusion	10.5/11/12 /14	RHS/I-sections	12 (12)	12
Wang and Wang (2016)	7A04-T6	Extrusion	-	Plates	2 (2)	2
Wang et al. (2013)	6082-T6	Extrusion	4/5/6/7/8/10 /12	SHS/RHS/I- /Angle sections	90 (90)	90
Yalçın and Genel (2019)	6063-T5	Extrusion	-	CHS	1 (0)	-
Yuan et al. (2015)	6061-T6/ 6063-T5	Extrusion	3.59-10.89	I-sections	48 (48)	48
Zha and Moen (2003)	6082-T6	Extrusion	5/6/8.5	Plates	3 (0)	-
Zhao et al. (2019)	6082-T6	Extrusion	4/5/6/7/8	SHS/CHS	5 (0)	-
Zhu and Young (2006)	6061-T6/ 6063-T5	Extrusion	1.6/3	CHS	4 (4)	4

Zhou and Young (2009)	6061-T6	Extrusion	2/2.5/3/4/5	CHS	10 (10)	10
Zhou and Young (2018)	6061-T6	Extrusion	2/2.5/3/4/5	CHS	6 (0)	-
Zhou and Young (2019)	6061-T6/ 6063-T5	Extrusion	1.4/1.9	Channel sections	4 (4)	4
Zhu et al. (2018)	6063-T5	Extrusion	4/5	I-sections	4 (0)	-
Zhu et al. (2019)	6061-T6/ 6063-T5	Extrusion	1.6/1.9	Lipped channel sections/Channel sections	4 (0)	4
Zhu et al. (2020)	6061-T6	Extrusion	10/14	I-sections/plate	2 (0)	-
Total					722 (473)	394

Table note: a. Specific aluminum alloy grade not provided; b. Values in brackets represent the number of cases in which the ultimate strain ε_u were provided.

The collected tensile coupon test results were reported to different levels of completeness, as summarized in Table 1, where the values in brackets represent the number of cases in which the ultimate strains ε_u were provided. Among the total of 722 tensile coupon tests, 394 tests were reported (or provided upon request) with their full stress-strain curves; these curves have been employed to derive appropriate values or predictive expressions for the strain hardening exponents n and m for the different aluminum alloy grades. The process by which all the required input parameters for the two-stage Ramberg-Osgood model (Mirambell and Real 2000) given by Eq. (4) were derived from the collected stress-strain data is described below, with particular attention given to the determination of the strain hardening exponents n and m.

Ordinary least squares (OLS) regression analysis, in which the sum of the squares of the differences between the measured strains $\varepsilon_{\text{mea,i}}$ and those predicted by the two-stage Ramberg-Osgood model $\varepsilon_{\text{R-O,i}}$ is minimized, was employed to determine the best fit n and m values for the 394 full stress-strain curves. The objective functions for n and m are given by Eqs. (6) and (7), respectively.

$$S(n) = Min\sum_{\text{i=1}}^{\text{k}}\left(\varepsilon_{\text{mea,i}} - \varepsilon_{\text{R-O,i}}\right)^2 = Min\sum_{\text{i=1}}^{\text{k}}\left[\varepsilon_{\text{mea,i}} - \left(\frac{f_{\text{i}}}{E} + 0.002\left(\frac{f_{\text{i}}}{f_{\text{y}}}\right)^n\right)\right]^2 \quad \text{for } 0 < \varepsilon_{\text{mea,i}} \le \varepsilon_{0.2} \quad (6)$$

$$S(m) = Min\sum_{i=1}^{k}\left(\varepsilon_{mea,i} - \varepsilon_{R\text{-}O,i}\right)^2$$
$$= Min\sum_{i=1}^{k}\left[\varepsilon_{mea,i} - \left(\frac{f_i - f_y}{E_{0.2}} + \left(\varepsilon_u - \varepsilon_{0.2} - \frac{f_u - f_y}{E_{0.2}}\right)\left(\frac{f_i - f_y}{f_u - f_y}\right)^m + \varepsilon_{0.2}\right)\right]^2 \quad \text{for } \varepsilon_{0.2} < \varepsilon_{mea,i} \le \varepsilon_u \qquad (7)$$

Since the strain rates are typically varied during coupon testing (Huang and Young 2014), the recorded data points are often not evenly distributed along the stress-strain curve, with higher concentrations of data lying in the region where a lower strain rate was applied (typically in the strain range between 0 and $\varepsilon_{0.2}$). Performing regression using the original stress-strain data points may, thus, result in biased estimates of the strain hardening exponents *n* and *m* towards the regions with higher concentrations of data. A further consideration is that anomalous results can be obtained in cases where the test stress-strain curves feature a high degree of experimental noise. To avoid the aforementioned problems, two polynomials, up to seventh order, were first fitted to the test stress-strain curves. The polynomial given by Eq. (8) with regression coefficients a_1 to a_7 was fitted to the initial part of the stress-strain curves, up to the yield strength $\varepsilon_{0.2}$, while Eq. (9), with regression coefficients b_1 to b_7 was used beyond this point.

$$f(\varepsilon) = \sum_{k=1}^{7} a_k \varepsilon^k \qquad \text{for } 0 \le \varepsilon \le \varepsilon_{0.2} \qquad (8)$$

$$f(\varepsilon) = f_y + \sum_{k=1}^{7} b_k (\varepsilon - \varepsilon_{0.2})^k \qquad \text{for } \varepsilon_{0.2} < \varepsilon \le \varepsilon_u \qquad (9)$$

The regression coefficients were determined using the software package MATLAB (MATLAB

2016); this process, as demonstrated in Fig. 4, enables the representation of the test stress-strain curves by continuous and smooth curves with explicit, yet complicated, functions (i.e. Eqs. (8) and (9)). The Young's modulus E, as well as other parameters of stresses and strains (including f_y, f_u, $\varepsilon_{0.2}$ and ε_u) employed in the two-stage Ramberg-Osgood model, can then be determined from the fitted polynomial curves, following the recommendations by Huang and Young (2014), and the strain hardening exponents n and m can be accurately captured by performing OLS regression analysis on the evenly distributed data points extracted from the polynomials.

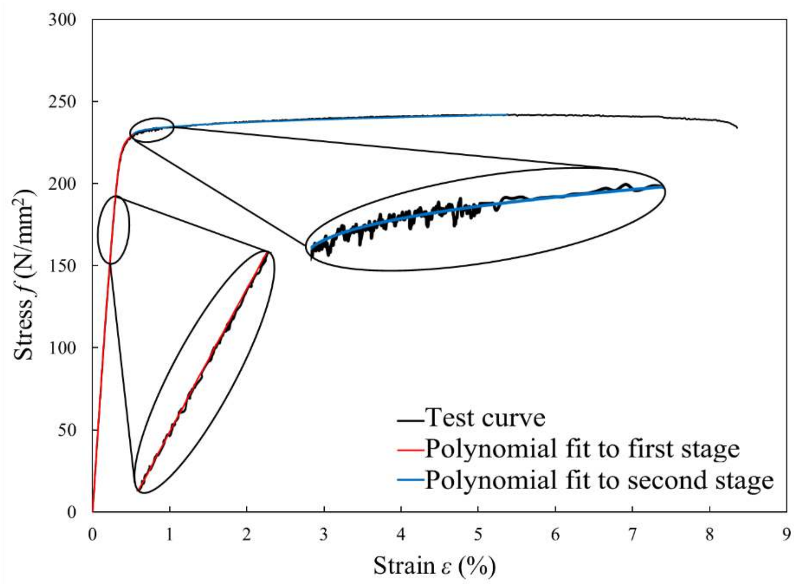

Fig. 4. Polynomial fitting to typical measured stress-strain curve

Results and discussion

Young's modulus E

The average Young's modulus values E determined from the collected data are presented in Table 2 and compared with those given in the European standard EN 1999-1-1:2007 (CEN 2007) and the American aluminum design manual (AA 2010). It can be seen that the code values represent the average measured values well, and that the measurements are generally very consistent with low coefficients of variation (COV). The results indicate a slightly higher Young's modulus for the grade 7A04-T6, though this is based on a relatively small number of coupon tests and requires further verification. Given the consistency of the results, the observation of no clear trend between the different aluminum alloys and considering simplicity and ease of use, a single Young's modulus value of 70,000 MPa, as adopted in EN 1999-1-1:2007 (CEN 2007) is recommended for all the investigated grades.

Table 2. Comparison of the average measured Young's modulus values with those provided in CEN (2007) and AA (2010) for different aluminum alloy grades

Aluminum alloy grade	No. of coupons with E provided	Average E MPa	COV	E (CEN 2007) MPa	E (AA 2010) MPa
5052-H36	218	69,500	0.014	70,000	70,300
6061-T6	113	68,800	0.049	70,000	69,600
6063-T5	31	68,400	0.050	70,000	69,600
6082-T6	103	69,700	0.035	70,000	69,600
7A04-T6	8	72,000	0.061	70,000	-

Strain at ultimate tensile strength ε_u

Annex E of EN 1999-1-1:2007 (CEN 2007), referred to as EC9, provides empirical expressions for the prediction of the strain at the ultimate tensile strength $\varepsilon_{u,EC9}$ for aluminum alloys, as given by Eqs. (10a) and (10b); the predictive expression for $\varepsilon_{u,EC9}$ depends only on the material yield strength f_y, which should be input in N/mm^2. The accuracy of the EC9 predictive model is assessed by comparing the 473 test results in which the ultimate strain $\varepsilon_{u,test}$ was reported (see Table 1) with their corresponding predicted values $\varepsilon_{u,EC9}$; the comparisons are presented in Fig. 5. It can be seen from Fig. 5 that the EC9 model generally yields significant over-predictions of the test values, with the mean value of the ratio of $\varepsilon_{u,test}/\varepsilon_{u,EC9}$ being 0.48 and the corresponding coefficient of variation (COV) being 0.303, as reported in Table 3.

$$\varepsilon_u = 0.3 - 0.22\left(f_y / 400\right) \quad \text{for } f_y < 400 \text{ N/mm}^2 \tag{10a}$$

$$\varepsilon_u = 0.08 \quad \text{for } f_y \geq 400 \text{ N/mm}^2 \tag{10b}$$

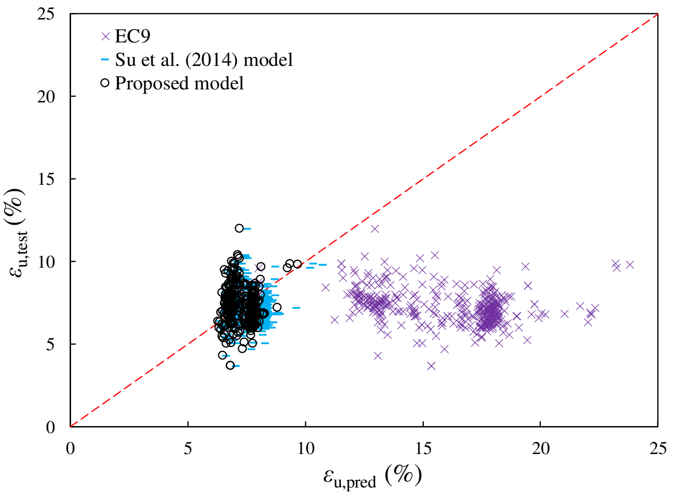

Fig. 5. Comparisons between test values of strain at ultimate strength $\varepsilon_{u,test}$ and those determined using different predictive models $\varepsilon_{u,pred}$

Table 3. Statistical evaluation of the accuracy of different predictive models for determining ε_u

	$\varepsilon_{u,test}/\varepsilon_{u,EC9}$	$\varepsilon_{u,test}/\varepsilon_{u,Su}$	$\varepsilon_{u,test}/\varepsilon_{u,prop}$
Mean	0.48	0.96	1.00
COV	0.303	0.178	0.163

To improve the accuracy of the EC9 predictive model, Su et al. (2014) proposed a new model for determining the ultimate strain $\varepsilon_{u,Su}$ for aluminum alloys, based on an expression similar in format to that developed for steel (Yun and Gardner 2017; Gardner and Yun 2018) and stainless steel (Rasmussen 2003; Arrayago et al. 2015), as given by Eq. (11).

$$\varepsilon_{u,Su} = 0.13\left(1 - f_y / f_u\right) + 0.06 \tag{11}$$

The accuracy of the Su et al. (2014) model is demonstrated in Fig. 5 and Table 3, as well as in Fig. 6 where the coupon test values of $\varepsilon_{u,test}$ are plotted against the corresponding ratios of f_y/f_u. This model can, however, be further improved based on the larger experimental database assembled in the present study, as shown in Fig. 6; the proposed modified predictive expression for $\varepsilon_{u,prop}$ is given by Eq. (12). As shown in Table 3, the mean value of $\varepsilon_{u,test}/\varepsilon_{u,prop}$ is equal to 1.00, with a COV of 0.163, revealing an improvement in terms of both accuracy and consistency over the Su et al. (2014) model.

$$\varepsilon_{\mathrm{u,prop}} = 0.1\left(1 - f_{\mathrm{y}} / f_{\mathrm{u}}\right) + 0.06 \tag{12}$$

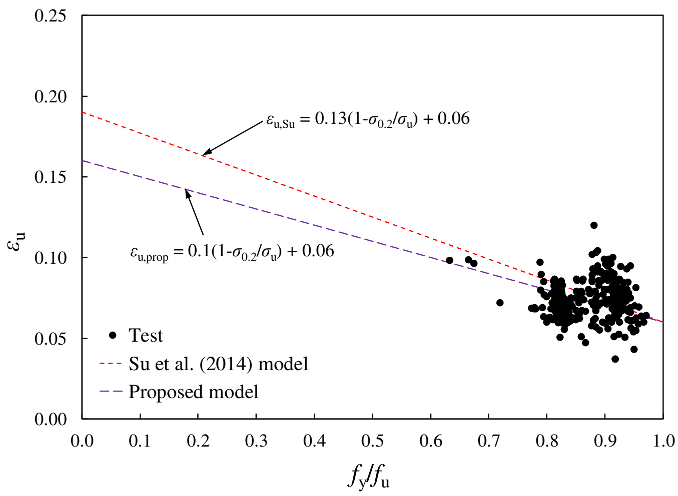

Fig. 6. Assessment of different predictive models for the strain at the ultimate tensile strength ε_u

Ultimate strength f_u

For instances in which the yield strength f_y is known (e.g. by measurement) but the ultimate strength f_u is not, a predictive expression for f_u is desirable. By analyzing the 722 collated coupon test results (summarized in Table 1), it was found that the aluminum alloy data follow a general trend of reducing ratios of f_u/f_y with increasing yield strength f_y, as shown in Fig. 7. Note that a similar trend between f_u/f_y and f_y has also been observed for carbon steels (Fukumoto 1996; Gardner and Yun 2018). The relationship between f_u/f_y and f_y for aluminum alloys can be represented by Eq. (13), which is a power law model with its coefficients of 60 and 1.5 chosen to fit the collated test results. The proposed predictive equation (Eq. (13)), in which f_y and f_u must be in N/mm^2, shows good agreement with the test results, with a mean value of the test-to-predicted ratios of f_u being 1.02 and a low corresponding COV of 0.044. It should be emphasized that the correlation between f_y and f_u depends largely on the work-hardened conditions (for non-heat-treatable aluminum alloys) or the heat treatment conditions (for heat-treatable aluminum alloys), thus the applicability of Eq. (13) for other aluminum alloy grades with different manufacturing conditions is yet to be further investigated.

$$f_u / f_y = 1 + \left(60/ f_y\right)^{1.5} \qquad (13)$$

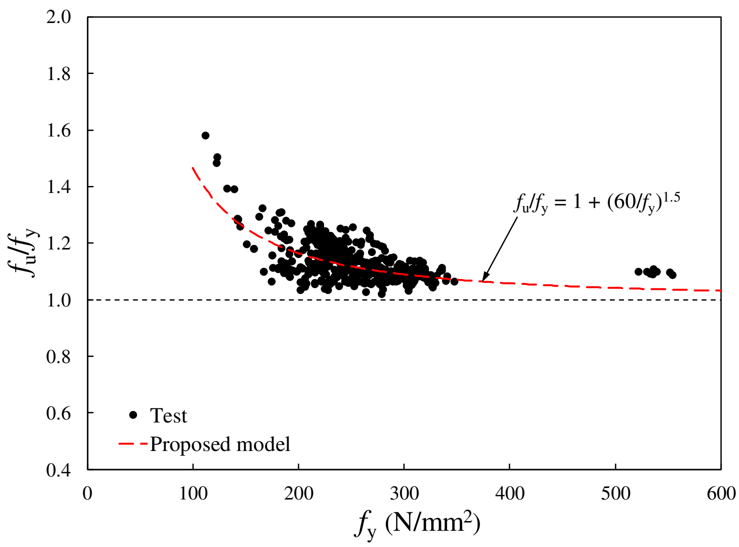

Fig. 7. Assessment of proposed predictive model for the ultimate strength f_u

Strain hardening exponent n

The first strain hardening exponent n employed in the two-stage Ramberg-Osgood model is conventionally determined for aluminum alloys using Eq. (2), forcing the curve to pass through, in addition to the 0.2% proof stress, a second reference point corresponding to the 0.1% proof stress $\sigma_{0.1}$, as shown in Fig. 3(a). It has been shown for cold-formed carbon steel (Gardner and Yun 2018) and stainless steel (Arrayago et al. 2015) that use of the 0.05% proof stress $\sigma_{0.05}$ yields more accurate estimates of n. Use of this alternative second reference point, which results in the definition of n given by Eq. (14), is now considered for aluminum alloys. The accuracy of the two predictive equations (Eqs. (2) and (14)) for aluminum alloys is assessed by comparing the test values n_{test}, determined from the collected full stress-strain curves by means of OLS regression analysis, as described above, with those predicted using Eqs. (2) and (14) (i.e. n_{pred}); the comparisons are shown in Fig. 8. It can be seen from Fig. 8 that Eq. (14) provides more accurate predictions of the n_{test} values than Eq. (2); this is further demonstrated by the statistical results presented in Table 4. The use of Eq. (14) is therefore recommended for the determination of the first strain hardening exponent n, provided that the 0.05% proof stress $\sigma_{0.05}$ is known. It is further recommended that this value is routinely reported in future experimental studies.

$$n = \frac{\ln(4)}{\ln\left(f_y / \sigma_{0.05}\right)} \quad (14)$$

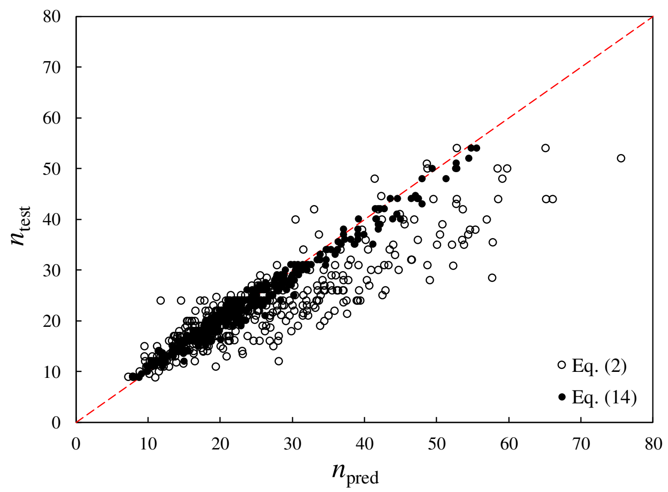

Fig. 8. Assessment of different predictive equations for the first strain hardening exponent n

Table 4. Statistical assessment of different predictive equations for the first strain hardening exponent n

	n_{test}/n_{pred}	
	Eq. (2)	Eq. (14)
Mean	0.92	1.00
COV	0.22	0.06

The degree of roundedness of the stress-strain curve approaching the yield strength is reflected by the value of the first strain hardening exponent n, with lower values signifying a more rounded response. The degree of nonlinearity depends mainly on the chemical composition of the material and the production process. Thus, as expected, the measured stress-strain curves for the same aluminum alloy grade display a similar degree of nonlinearity, making the parameter n grade specific. A summary of the average n values for the five investigated structural aluminum alloy grades is provided in Table 5. It can be observed that the fully heat-treated aluminum alloys (i.e. 6061-T6, 6082-T6 and 7A04-T6) tend to exhibit the higher values of n, corresponding to the stress-strain curves displaying a sharper yield point. Adoption of these average n values is recommended when the value of $\sigma_{0.05}$ is not available and hence Eq. (14) cannot be applied. The average values from the collected coupon test results of the other key material parameters, including E, f_y, f_u and ε_u, are also listed in Table 5.

Table 5. Summary of average measured values of the basic material parameters used for two-stage Ramberg-Osgood model for studied aluminum alloy grades

Aluminum alloy grade	No. of full stress-strain curves	E N/mm^2	f_y N/mm^2	f_u N/mm^2	ε_u	n	m
5052-H36	146	69,700	220	270	0.07	16	2.5
6061-T6	103	69,100	250	280	0.07	24	2.5
6063-T5	40	69,000	160	200	0.08	15	2.6
6082-T6	97	69,700	300	330	0.08	26	2.2
7A04-T6	8	72,000	540	590	0.08	33	2.3

Strain hardening exponent m

Analogous to the approach used to determine the first strain hardening exponent n, the second strain hardening exponent m can be calculated by forcing the second stage of the two-stage Ramberg-Osgood model to pass through an intermediate reference point between ($\varepsilon_{0.2}$, f_y) and (ε_u, f_u). Considering the point corresponding to either the 1% proof stress $\sigma_{1.0}$ or the 2% proof stress $\sigma_{2.0}$ as the intermediate reference point results in Eq. (15) and Eq. (16), respectively, for the determination of m (Quach and Huang 2011; Gardner and Yun 2018). Both equations provide good estimates of the test values m_{test}, which were determined using the aforementioned data processing approach, as shown in Fig. 4. Of the two equations, Eq. (15) is recommended because $\sigma_{1.0}$ is more likely to be reported by researchers and manufacturers, but in many cases, the measured values of neither $\sigma_{1.0}$ nor $\sigma_{2.0}$ will be available, preventing the use of either Eq. (15) or Eq. (16). It is thus desirable to provide representative average values for m to capture the degree of nonlinearity of the second stage of stress-strain curves for aluminum alloys.

$$m=\frac{\ln\left(0.008+\frac{\sigma_{1.0}-f_y}{E}-\frac{\sigma_{1.0}-f_y}{E_{0.2}}\right)-\ln\left(\varepsilon_u-\varepsilon_{0.2}-\frac{f_u-f_y}{E_{0.2}}\right)}{\ln\left(\sigma_{1.0}-f_y\right)-\ln(f_u-f_y)} \tag{15}$$

$$m=\frac{\ln\left(0.018+\frac{\sigma_{2.0}-f_y}{E}-\frac{\sigma_{2.0}-f_y}{E_{0.2}}\right)-\ln\left(\varepsilon_u-\varepsilon_{0.2}-\frac{f_u-f_y}{E_{0.2}}\right)}{\ln\left(\sigma_{2.0}-f_y\right)-\ln(f_u-f_y)} \tag{16}$$

The second strain hardening exponent m has been found to be related to the ratio of yield to ultimate strength f_y/f_u for cold-formed carbon steel (Gardner and Yun 2018) and stainless steel (Rasmussen 2003; Arrayago et al. 2015), but this correlation is not seen for aluminum alloys, as shown in Fig. 9, where the values of m_{test} are plotted against their corresponding ratios of f_y/f_u, grouped by aluminum alloy grade. This is because, for heat-treatable aluminum alloys, the strain hardening level (reflected by the second strain hardening exponent m) may also vary with temper of the alloy, which, for the same aluminum alloy grade, the higher tempered alloy generally shows a less pronounced of strain hardening compared to that of the lower tempered alloy. This is also reflected by the characteristic values of the exponent n EC9 (CEN 2007). Although there are no clear trends in the m_{test} data, the range of values is small, with the majority of data falling between 2.0 and 3.0. The average m_{test} values for each aluminum alloy grade are reported in Table 5, while, for simplicity, an overall average value of 2.4 may be used.

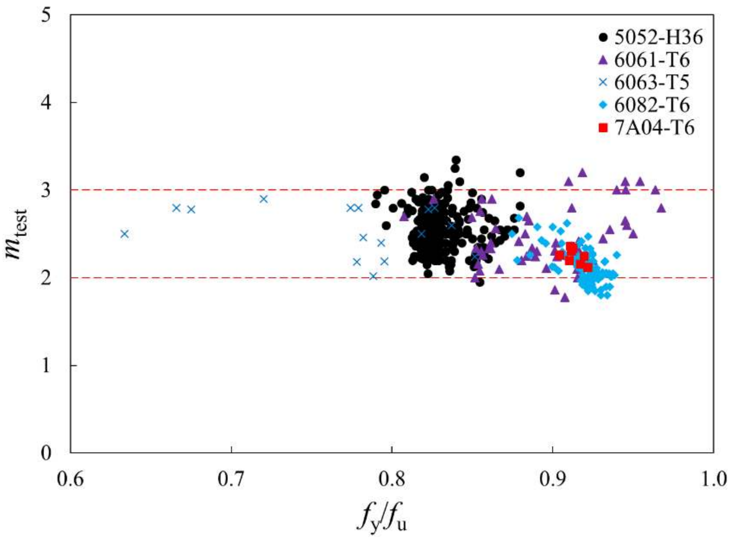

Fig. 9. Relationship between m_{test} and f_y/f_u

Comparison with experimental stress-strain curves

The accuracy of the proposed two-stage Ramberg-Osgood model for aluminum alloys, as described above, is assessed by comparing a series of predicted curves with the corresponding experimental stress-strain curves. Five representative comparisons, one for each aluminum alloy grade, are presented in Figs. 10-14. The two-stage Ramberg-Osgood curves illustrated in Figs. 10-14 utilize the measured values of the key input parameters − E, f_y, f_u, ε_u, n and m for each respective aluminum alloy coupon test, as summarized in Table 6. Stress-strain curves generated from the single-stage Ramberg-Osgood model, with the strain hardening exponent n determined from either Eq. (2) or Eq. (3), are also plotted in Figs. 10-14 for comparison purposes. Note that the predicted curves from the single-stage Ramberg-Osgood model, with n calculated from Eq. (2), are terminated when the stress reaches the measured ultimate strength f_u. It can be seen from Figs. 10-14 that the single-stage Ramberg-Osgood model with n calculated using Eq. (2) fails to capture the full-range stress strain response of aluminum alloys, except for the 7A04-T6 grade, while the single-stage Ramberg-Osgood model with n calculated using Eq. (3) provides a good overall description of the experimental stress-strain curves but loses accuracy in the important initial yielding region, as highlighted in Figs. 10(b) to 14(b).

The two-stage Ramberg-Osgood model, on the other hand, provides an accurate description of the experimental stress-strain curves over the full range of strains up to ε_u.

Table 6. Key measured material properties of the selected aluminum alloy coupon tests used for comparisons with predicted stress-strain curves

Source	Aluminum alloy grade	Coupon label	E N/mm^2	f_y N/mm^2	f_u N/mm^2	ε_u %	n_{test}	m_{test}
Huynh et al. (2019)	5052-H36	C40030_LT_F04_1	69,400	232	270	6.10	12	2.8
Su et al. (2015)	6061-T6	H50×95×10.5B5II	70,200	192	222	8.54	15	2.9
Su et al. (2014)	6063-T5	+N95×50×10.5C	70,400	151	181	7.32	10	2.6
Wang et al. (2013)	6082-T6	H3-2	66,500	322	349	7.49	25	2.0
Wang et al. (2016a)	7A04-T6	L100-8-2	69,550	533	582	6.98	33	2.2

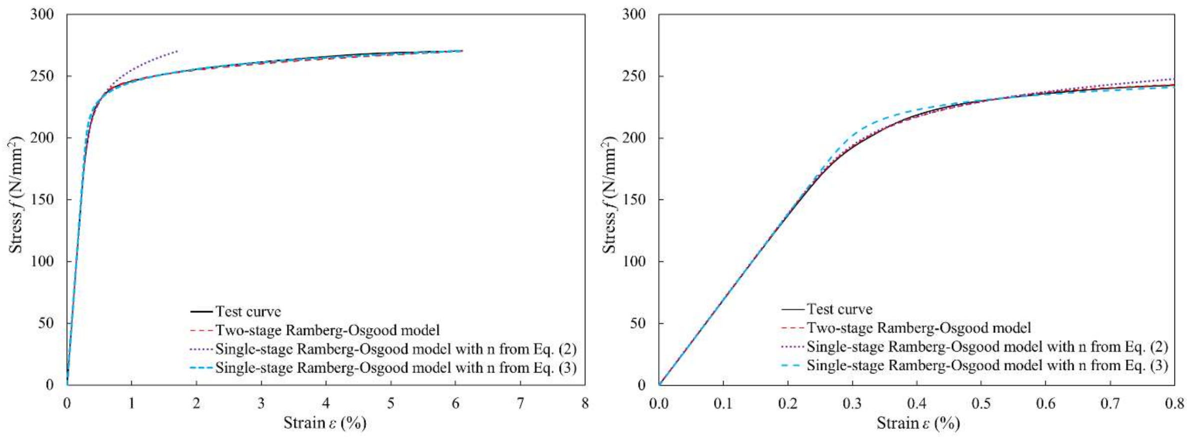

(a) Full stress-strain curves (b) Stress-strain curves up to 0.8% strain

Fig. 10. Comparison of different material models with an experimental stress-strain curve on grade 5052-H36 aluminum alloy reported by Huynh et al. (2019)

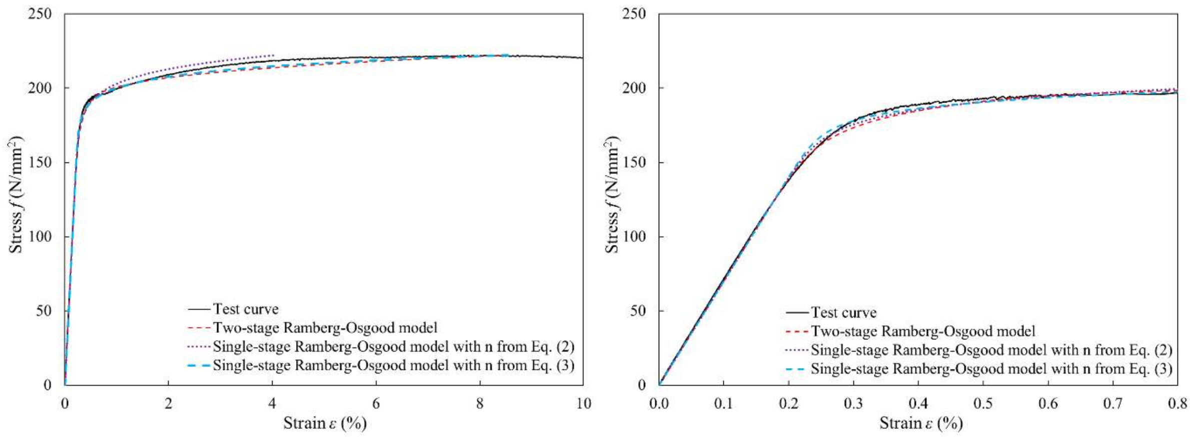

(a) Full stress-strain curves (b) Stress-strain curves up to 0.8% strain

Fig. 11. Comparison of different material models with an experimental stress-strain curve on grade 6061-T6 aluminum alloy reported by Su et al. (2015)

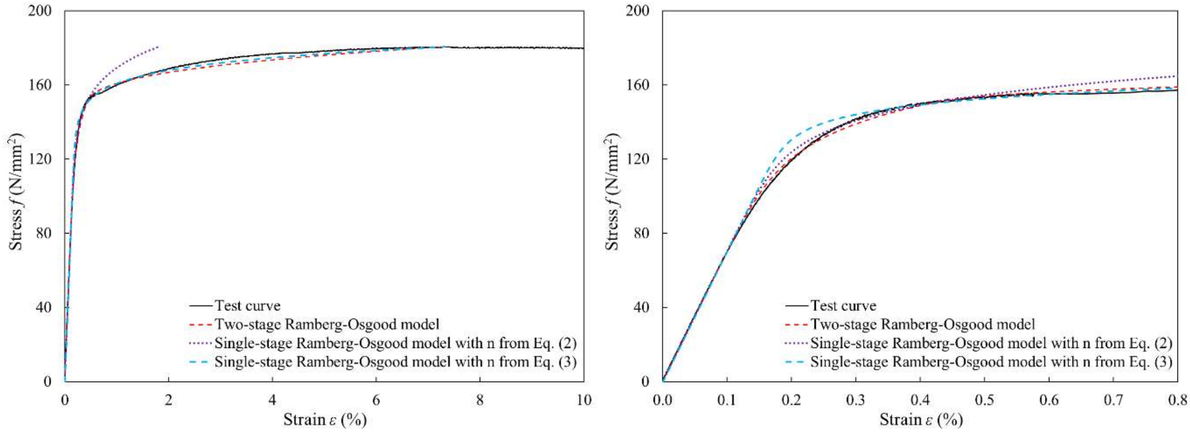

(a) Full stress-strain curves (b) Stress-strain curves up to 0.8% strain

Fig. 12. Comparison of different material models with an experimental stress-strain curve on grade 6063-T5 aluminum alloy reported by Su et al. (2014)

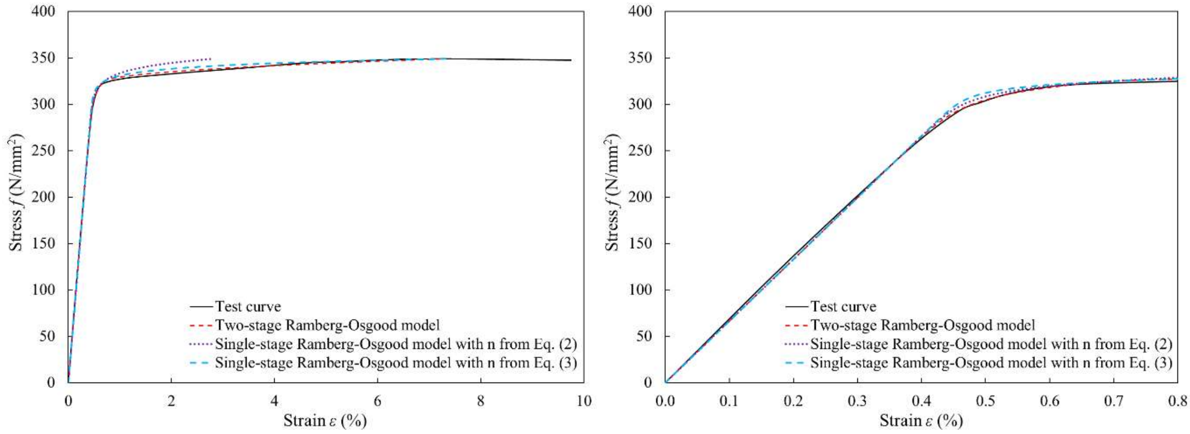

(a) Full stress-strain curves (b) Stress-strain curves up to 0.8% strain

Fig. 13. Comparison of different material models with an experimental stress-strain curve on grade 6082-T6 aluminum alloy reported by Wang et al. (2013)

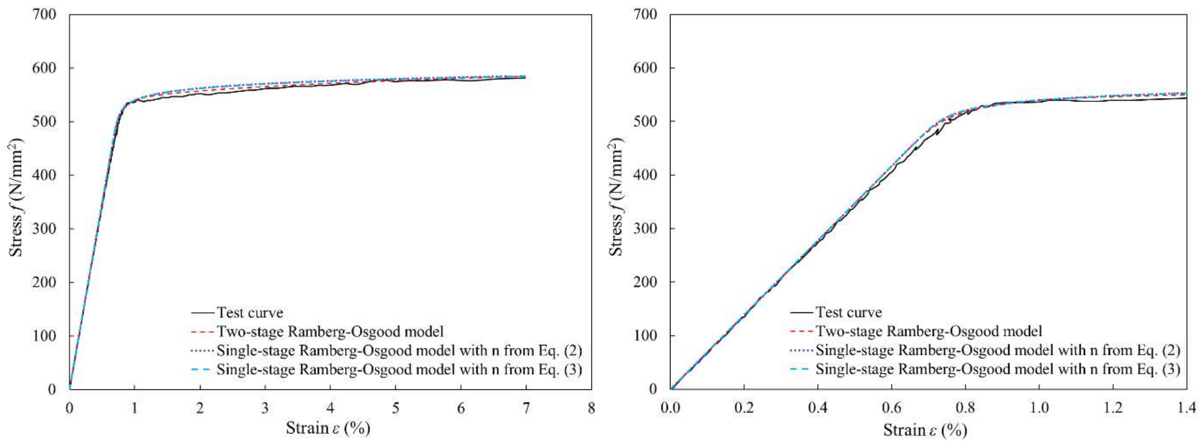

(a) Full stress-strain curves (b) Stress-strain curves up to 1.4% strain

Fig. 14. Comparison of different material models with an experimental stress-strain curve on grade 7A04-T6 aluminum alloy reported by Wang et al. (2016a)

The accuracy of the proposed two-stage Ramberg-Osgood model with different levels of assumed knowledge of availability of the key input parameters is also assessed. Three cases are considered. In Case 1, it is assumed that the measured values of E, f_y, f_u and ε_u are known and n and m are taken as the average values given in Table 5. In Case 2, it is assumed that the measured values of E, f_y and f_u are known, ε_u is predicted using Eq. (12), and the average values of n and m from Table 5 are used. In Case 3, it is assumed that only the measured value of f_y is known, E is assigned the recommended value of 70,000 N/mm^2, ε_u and f_u are predicted using Eqs. (12) and (13), respectively, and the average values of n and m from Table 5 are used. The five previously selected coupon tests (see Table 6) are used for this demonstration; the comparisons are shown in Figs. 15-19.

The proposed two-stage Ramberg-Osgood model can be seen to generally provide an accurate representation of the experimental stress-strain curves, especially when greater knowledge of the material input parameters is assumed (i.e. moving from Case 3 to Case 1). Typically, the nominal or measured values of the three key material properties E, f_y and f_u are readily available e.g. from material specifications, design standards or experimental reports; this corresponds to Case 2 of the described comparisons. For this scenario, the predicted two-stage Ramberg-Osgood curves are shown to yield consistently accurate representations of the experimental stress-strain curves, as depicted by the purple dotted lines in Figs. 15-19.

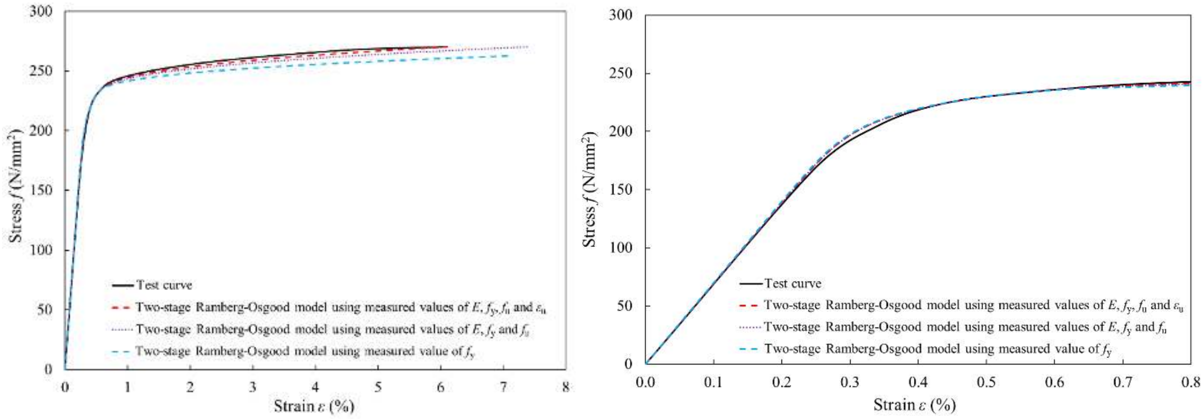

(a) Full stress-strain curves (b) Stress-strain curves up to 0.8% strain

Fig. 15. Comparison of the predicted two-stage Ramberg-Osgood curves based on different measured material parameters with an experimental stress-strain curve on grade 5052-H36 aluminum alloy reported by Huynh et al. (2019)

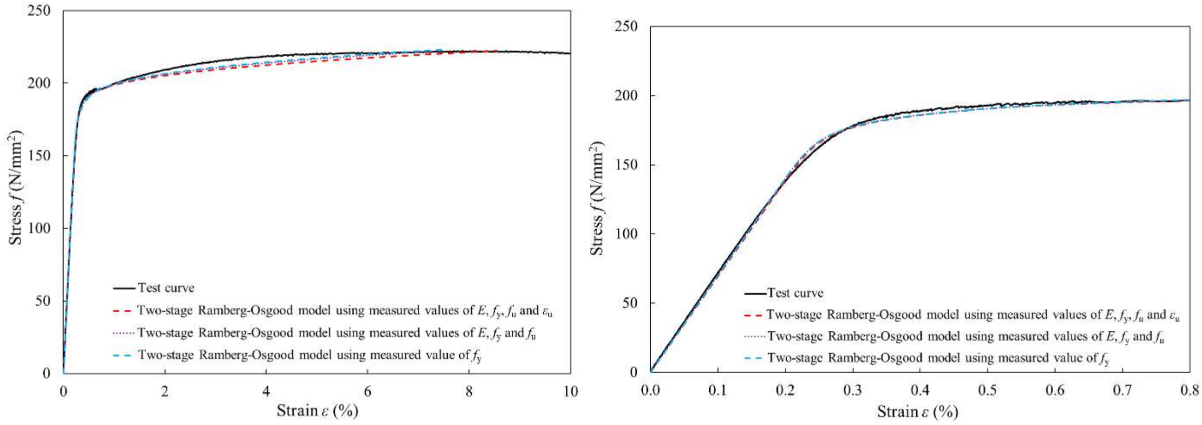

(a) Full stress-strain curves (b) Stress-strain curves up to 0.8% strain

Fig. 16. Comparison of the predicted two-stage Ramberg-Osgood curves based on different measured material parameters with an experimental stress-strain curve on grade 6061-T6 aluminum alloy reported by Su et al. (2015)

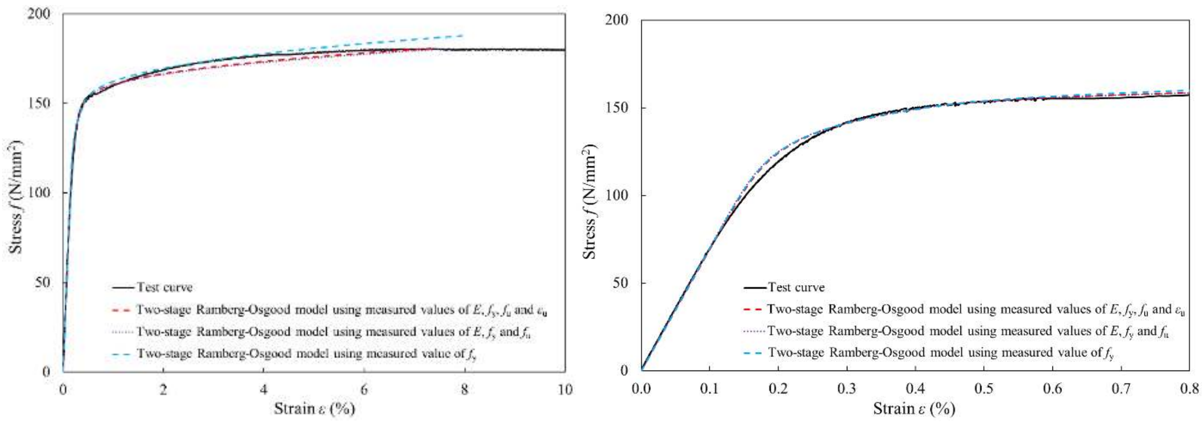

(a) Full stress-strain curves (b) Stress-strain curves up to 0.8% strain

Fig. 17. Comparison of the predicted two-stage Ramberg-Osgood curves based on different measured material parameters with an experimental stress-strain curve on grade 6063-T5 aluminum alloy reported by Su et al. (2014)

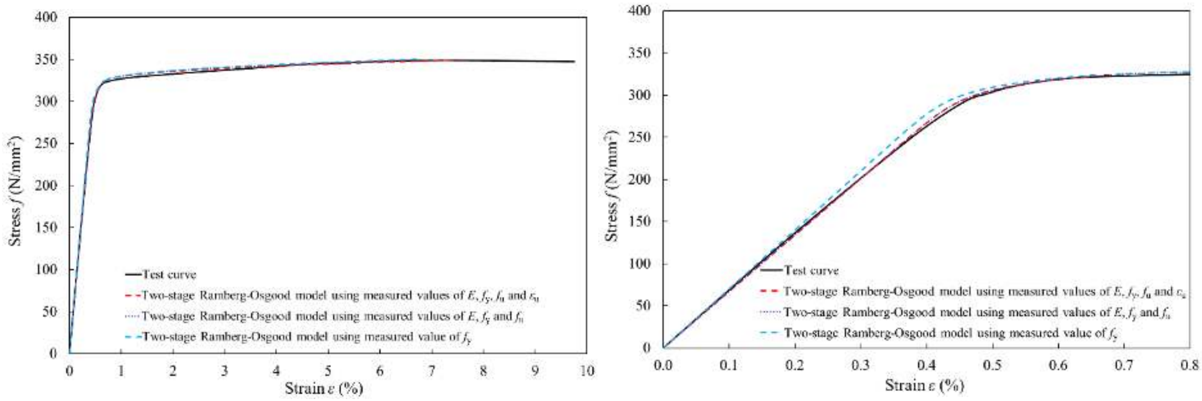

(a) Full stress-strain curves (b) Stress-strain curves up to 0.8% strain

Fig. 18. Comparison of the predicted two-stage Ramberg-Osgood curves based on different measured material parameters with an experimental stress-strain curve on grade 6082-T6 aluminum alloy reported by Wang et al. (2013)

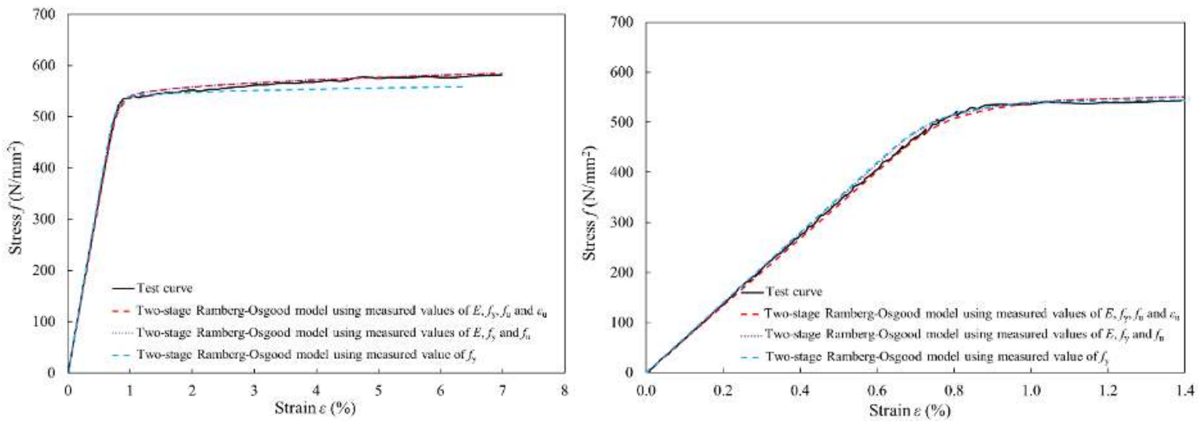

(a) Full stress-strain curves (b) Stress-strain curves up to 1.4% strain

Fig. 19. Comparison of the predicted two-stage Ramberg-Osgood curves based on different measured material parameters with an experimental stress-strain curve on grade 7A04-T6 aluminum alloy reported by Wang et al. (2016a)

Summary of the proposed model

The proposed two-stage Ramberg-Osgood model, along with the recommended values and predictive expressions for the key input parameters, for describing the stress-strain relationship of aluminum alloys is summarized in this section. The general form of the model is given as follows:

$$\varepsilon = \begin{cases} \dfrac{f}{E} + 0.002\left(\dfrac{f}{f_{\mathrm{y}}}\right)^{n}, & \text{for } 0 < f \le f_{\mathrm{y}} \\ \dfrac{f - f_{\mathrm{y}}}{E_{0.2}} + \left(\varepsilon_{\mathrm{u}} - \varepsilon_{0.2} - \dfrac{f_{\mathrm{u}} - f_{\mathrm{y}}}{E_{0.2}}\right)\left(\dfrac{f - f_{\mathrm{y}}}{f_{\mathrm{u}} - f_{\mathrm{y}}}\right)^{m} + \varepsilon_{0.2}, & \text{for } f_{\mathrm{y}} < f \le f_{\mathrm{u}} \end{cases} \tag{4}$$

where:

E is the Young's modulus that may be taken as 70,000 N/mm^2 or as the average value per grade from Table 5;

$E_{0.2}$ is the tangent modulus of the stress-strain curve at the yield strength f_y defined by Eq. (5);

$$E_{0.2} = \frac{E}{1 + 0.002n\dfrac{E}{f_y}} \quad (5)$$

$\varepsilon_{0.2}$ is the total strain at the yield strength which equals to $f_y/E + 0.002$;

ε_u is the strain at the ultimate tensile strength f_u that can be determined by Eq. (12); for cases where f_u is not available, it may be estimated from Eq. (13), in which f_y and f_u are in N/mm^2;

$$\varepsilon_u = 0.1\left(1 - f_y / f_u\right) + 0.06 \quad (12)$$

$$f_u / f_y = 1 + \left(60/f_y\right)^{1.5} \quad (13)$$

n is the first strain hardening exponent that may be taken from Table 5 or determined from Eq. (14) when the measured 0.05% proof stress $\sigma_{0.05}$ is available;

$$n = \frac{\ln(4)}{\ln\left(f_y/\sigma_{0.05}\right)} \quad (14)$$

m is the second strain hardening exponent that may be taken from Table 5 or calculated from Eq. (15), which requires knowledge of the measured 1% proof stress.

$$m = \frac{\ln\left(0.008 + \frac{\sigma_{1.0} - f_{\mathrm{y}}}{E} - \frac{\sigma_{1.0} - f_{\mathrm{y}}}{E_{0.2}}\right) - \ln\left(\varepsilon_{\mathrm{u}} - \varepsilon_{0.2} - \frac{f_{\mathrm{u}} - f_{\mathrm{y}}}{E_{0.2}}\right)}{\ln\left(\sigma_{1.0} - f_{\mathrm{y}}\right) - \ln(f_{\mathrm{u}} - f_{\mathrm{y}})} \tag{15}$$

It should be noted that the two-stage Ramberg-Osgood model is developed to describe the engineering (nominal) stress-strain curve, while, up to the ultimate tensile strength f_{u}, the curve can be converted to true stress-strain curve using the following two equations:

$$f_{\mathrm{true}} = f(1 + \varepsilon) \tag{17}$$

$$\varepsilon_{\mathrm{true}} = \ln(1 + \varepsilon) \tag{18}$$

where f_{ture} and $\varepsilon_{\mathrm{ture}}$ are true stress and true strain respectively.

Conclusions

A comprehensive study into the constitutive modeling of aluminum alloys has been presented. The two-stage Ramberg-Osgood model, originally proposed by Mirambell and Real (2000) for stainless steels, has been adopted in the present study to describe the nonlinear stress-strain behavior of aluminum alloys. Values and predictive expressions for the key input parameters of the two-stage Ramberg-Osgood expression have been developed based on the analysis of an assembled experimental database comprising a total of 722 coupon test results, with a focus on five aluminum alloy grades that are commonly used in structural applications, namely 5052-H36, 6061-T6, 6063-T5, 6082-T6 and 7A04-T6. It has been shown that the proposed model provides a very accurate representation of experimental stress-strain curves over the full range of tensile strains up to the ultimate tensile strain, especially when at least the three fundamental material parameters – the Young's modulus E, the yield strength f_{y} and the ultimate strength f_{u}

– are known. The proposed model presented herein is considered suitable for use in advanced numerical simulations and design methods, particularly in instances where large plastic strains are encountered.

Dada Availability Statement

Some or all data, models, or code that support the findings of this study are available from the corresponding author upon reasonable request.

Acknowledgement

The authors would like to thank Dr. Mei-Ni Su from the University of Manchester, Dr. Feng Zhou from Tongji University, Prof. Jihua Zhu from Shenzhen University, Dr. Cao Hung Pham from the University of Sydney and Prof. Yuanqing Wang from Tsinghua University for the provision of experimental stress-strain curves.

References

Aalberg, A. (2015). "Design of aluminium beam ends with flange copes." *Thin-Walled Struct.*, 94, 593-602.

AA (Aluminum Association). (2010). "Aluminum design manual." Washington, DC.

Alsanat, H., Gunalan, S., Guan, H., Keerthan, P., and Bull, J. (2019). "Experimental study of aluminium lipped channel sections subjected to web crippling under two flange load cases." *Thin-Walled Struct.*, 141, 460-476.

AS (Australian Standard). (2007). "Metallic materials – tensile testing at ambient temperature." *AS 1391-2007,* Sydney, Australia.

ASTM (American Society for Testing and Materials). (2013). "Standard test methods for tension testing of metallic materials." *E8/E8M-15a,* West Conshohocken, USA.

Arrayago, I., Real, E., and Gardner, L. (2015). "Description of stress-strain curves for stainless steel alloys." *Mater. Des.*, 87, 540-552.

Baehre, R. (1966). *Trycktastravorav elastoplastikt material-nagrafragestallninga*. (*Comparison between structural behaviour of elastoplastic material*). Report No. 16, Tekn. De Arne Johnson Ingenjorsbyra. (in German).

Brando, G., Sarracco, G., and De Matteis, G. (2015). "Strength of an aluminum column web in tension." *J. Struct. Eng.*, 141(7), 04014180.

CEN (European Committee for Standardization). (2007). "Eurocode 9: Design of aluminum structures – Part 1-1: General rules – General rules and rules for buildings." *BS EN 1999-1-1:2007*, Brussels.

CEN (European Committee for Standardization). (2009). "Metallic materials – Tensile testing – Part 1: Method of test at ambient temperature" *BS EN ISO 6892-1*, Brussels.

Chen, W., Deng, H., Dong, S., and Zhu, Z. (2018). "Numerical modelling of lockbolted lap connections for aluminium alloy plates." *Thin-Walled Struct.*, 130, 1-11.

Chen, Y., Feng, R., and Xu, J. (2017). "Flexural behaviour of CFRP strengthened concrete-filled aluminium alloy CHS tubes." *Constr. Build. Mater.*, 142, 295-319.

Chen, Y., Li, M., Yang, X., and Luo, W. (2020). "Damage and failure characteristics of CFRP/aluminum single lap joints designed for lightweight applications." *Thin-Walled Struct.*, 153, 106802.

Cho, Y., and Kim, T. (2016). "Estimation of ultimate strength in single shear bolted connections with aluminum alloys (6061-T6)." *Thin-Walled Struct.*, 101, 43-57.

Davies, A. W., and Roberts, T. M. (1999). "Resistance of welded aluminum alloy plate girders to shear and patch loading." *J. Struct. Eng.*, 125(8), 930-938.

De Matteis, G., Mandara, A., and Mazzolani, F. M. (2000). "T-stub aluminium joints: influence of behavioural parameters." *Comput. Struct.*, 78(1–3), 311-327.

Dwight, J. (1998). *Aluminium design and construction*, E & FN Spon, London.

Dundu, M. (2018). “Evolution of stress–strain models of stainless steel in structural engineering applications.” *Constr. Build. Mater.*, 165, 413-423.

Đuričić, Đ., Aleksić, S., Šćepanović, B., and Lučić, D. (2017). “Experimental, theoretical and numerical analysis of K-joint made of CHS aluminium profiles.” *Thin-Walled Struct.*, 119, 58-71.

Faella, C., Mazzolani, F. M., Piluso, V., and Rizzano, G. (2000). “Local buckling of aluminum members: testing and classification.” *J. Struct. Eng.*, 126(3), 353-360.

Fieber, A., Gardner, L., and Macorini, L. (2020). “Structural steel design using second-order inelastic analysis with strain limits.” *J. Constr. Steel Res.*, 168, 105980.

Feng, R., and Young, B. (2015). “Experimental investigation of aluminum alloy stub columns with circular openings.” *J. Struct. Eng.*, 141(11), 04015031.

Feng, R., Sun, W., Shen, C., and Zhu, J. (2017). “Experimental investigation of aluminum square and rectangular beams with circular perforations.” *Eng. Struct.*, 151, 613-632.

Feng, R., Zhu, W., Wan, H., Chen, A., and Chen, Y. (2018). “Tests of perforated aluminium alloy SHSs and RHSs under axial compression.” *Thin-Walled Struct.*, 130, 194-212.

Feng, R., Chen, Z., Shen, C., Roy, K., Chen, B., and Lim, J. B. (2020). “Flexural capacity of perforated aluminium CHS tubes – An experimental study.” *Structures*, 25, 463-480.

Fukumoto, Y. (1996). “New constructional steels and structural stability.” *Eng. Struct.*, 18(10), 786-791.

Gardner, L., and Ashraf, M. (2006). “Structural design for non-linear metallic materials.” *Eng. Struct.*, 28, 926-934.

Gardner, L., Insausti, A., Ng, K. T., and Ashraf, M. (2010). “Elevated temperature material properties of stainless steel alloys.” *J. Constr. Steel Res.*, 66(5), 634-647.

Gardner, L., Bu, Y., Francis, P., Baddoo, N. R., Cashell, K. A., and McCann, F. (2016). "Elevated temperature material properties of stainless steel reinforcing bar." *Constr. Build. Mater.*, 114, 977-997.

Gardner, L., and Yun, X. (2018). "Description of stress-strain curves for cold-formed steels." *Constr. Build. Mater.*, 189, 527-538.

Gardner, L. (2019). "Stability and design of stainless steel structures – Review and outlook." *Thin-Walled Struct.*, 141, 208-216.

Gardner, L., Yun, X., Fieber, A., and Macorini, L. (2019). "Steel design by advanced analysis: material modeling and strain limits." *Engineering*, 5(2), 243-249.

Guo, X. N. (2006). "Theoretical and experimental research on the aluminum alloy structure members." Ph.D. thesis, College of Civil Engineering, Tongji Univ., Shanghai, China. (in Chinese).

Guo, X. N., Tao, L., Zhu, S., and Zong, S. (2020). "Experimental investigation of mechanical properties of aluminum alloy at high and low temperatures." *J. Mater. Civil Eng.*, 32(2), 06019016.

He, L., Liu, C., Wu, Z., and Yuan, J. (2019). "Stability analysis of an aluminum alloy assembly column in a modular support structure." *Thin-Walled Struct.*, 135, 548-559.

Hill, H. N. (1944). *Determination of stress-strain relations from the offset yield strength values*. Technical Note No. 927, National Advisory Committee for Aeronautics, Washington, D.C., USA.

Hopperstad, O. S., Langseth, M., and Tryland, T. (1999). "Ultimate strength of aluminium alloy outstands in compression: experiments and simplified analysis." *Thin-Walled Struct.*, 34(4), 279-294.

Hradil, P., Talja, A., Real, E., Mirambell, E., and Rossi, B. (2013). "Generalized multistage mechanical model for nonlinear metallic materials." *Thin-Walled Struct.*, 63, 63-69.

Huynh, L. A. T., Pham, C. H., and Rasmussen, K. J. R. (2019). "Mechanical properties and residual stresses in cold-rolled aluminium channel sections." *Eng. Struct.*, 199, 109562.

Huang, Y., and Young, B. (2014). "The art of coupon tests." *J. Constr. Steel Res.*, 96, 159-175.

Islam, S. Z., and Young, B. (2012). "Web crippling of aluminium tubular structural members strengthened by CFRP." *Thin-Walled Struct.*, 59, 58-69.

Jiang, Y., Ma, H., Liew, J. R., and Fan, F. (2020). "Testing of aluminum alloyed bolted joints for connecting aluminum rectangular hollow sections in reticulated shells." *Eng. Struct.*, 218, 110848.

Jiang, S., Xiong, Z., Guo, X., and He, Z. (2018). "Buckling behaviour of aluminium alloy columns under fire conditions." *Thin-Walled Struct.*, 124, 523-537.

Kim, T., and Cho, Y. (2014). "Investigation on ultimate strength and failure mechanism of bolted joints in two different aluminum alloys." *Mater. Des.*, 58, 74-88.

Liu, M., Zhang, L., Wang, P., and Chang, Y. (2015). "Buckling behaviors of section aluminum alloy columns under axial compression." *Eng. Struct.*, 95, 127-137.

Liu, H., Ying, J., Meng, Y., and Chen, Z. (2019a). "Flexural behavior of double-and single-layer aluminum alloy gusset-type joints." *Thin-Walled Struct.*, 144, 106263.

Liu, Y., Liu, H., and Chen, Z. (2019b). "Post-fire mechanical properties of aluminum alloy 6082-T6." *Constr. Build. Mater.*, 196, 256-266.

Mazzolani, F. M. (1972). "Characterization of the σ–ε law and buckling of aluminum columns." *Constr. Metal*, 3.

Mazzolani, F. M. (1995). *Aluminium alloy structures*, 2nd Ed., E & FN Spon, London.

Mazzolani, F. M., Piluso, V., and Rizzano, G. (2011). "Local buckling of aluminum alloy angles under uniform compression." *J. Struct. Eng.*, 137(2), 173-184.

May, J. E., and Menzemer, C. C. (2005). "Strength of bolted aluminum alloy tension members." *J. Struct. Eng.*, 131(7), 1125-1134.

Ma, H., Jiang, Y., Li, C., Yu, Z., and Fan, F. (2020). "Performance analysis and comparison study of two aluminum alloy joint systems under out-of-plane and in-plane loading. An experimental and numerical investigation." *Eng. Struct.*, 214, 110643.

Mirambell, E., and Real, E. (2000). "On the calculation of deflections in structural stainless steel beams: an experimental and numerical investigation." *J. Constr. Steel Res.*, 54(1), 109-133.

MATLAB. (2016). The Mathworks, Inc, Natick, Mass, USA.

Quach, W. M., Teng, J. G., and Chung, K. F. (2008). "Three-stage full-range stress-strain model for stainless steels." *J. Struct. Eng.*, 134(9), 1518-1527.

Quach, W. M., and Huang, J. F. (2011). "Stress-strain models for light gauge steels." *Procedia Eng.*, 14, 288-296.

Ramberg, W., and Osgood, W. R. (1943). *Description of stress-strain curves by three parameters*. Technical Note No. 902, National Advisory Committee for Aeronautics, Washington, D.C., USA.

Rasmussen, K. J. R. (2003). "Full-range stress-strain curves for stainless steel alloys." *J. Constr. Steel Res.*, 59(1), 47-61.

Rouholamin, M., Gunalan, S., Poologanathan, K., and Karampour, H. (2020). "Experimental study of roll-formed aluminium lipped channel beams in shear." *Thin-Walled Struct.*, 153, 106687.

Rønning, L., Aalberg, A., and Larsen, P. K. (2010). "An experimental study of ultimate compressive strength of transversely stiffened aluminium panels." *Thin-Walled Struct.*, 48(6), 357-372.

Shi, M., Xiang, P., and Wu, M. (2018). "Experimental investigation on bending and shear performance of two-way aluminum alloy gusset joints." *Thin-Walled Struct.*, 122, 124-136.

Spyrakos, C. C., and Ermopoulos, J. (2005). “Development of aluminum load-carrying space frame for building structures.” *Eng. Struct.*, 27(13), 1942-1950.

Standards Australia. (1997). “Aluminum structures part 1: Limit state design.” *AS/NZS 1664.1:1997*, Sydney, Australia.

Su, M. N., Young, B., and Gardner, L. (2014). “Testing and design of aluminum alloy cross sections in compression.” *J. Struct. Eng.*, 140(9), 04014047.

Su, M. N., Young, B., and Gardner, L. (2015). “Continuous beams of aluminum alloy tubular cross sections. I: tests and FE model validation.” *J. Struct. Eng.*, 141(9), 04014232.

Su, M. N., and Young, B. (2019). “Material properties of normal and high strength aluminium alloys at elevated temperatures.” *Thin-Walled Struct.*, 137, 463-471.

Tajeuna, T. A., Légeron, F., Labossière, P., Demers, M., and Langlois, S. (2015). “Effect of geometrical parameters of aluminum-to-steel bolted connections.” *Eng. Struct.*, 102, 344-357.

Tryland, T., Langseth, M., and Hopperstad, O. S. (1999). “Nonperfect aluminum beams subjected to concentrated loading.” *J. Struct. Eng.*, 125(8), 900-909.

Wang Y. J., Fan, F., Qian, H., and Zhai, X. M. (2013). “Experimental study on constitutive model of high-strength aluminum alloy 6082-T6.” *J. Build. Struct.*, 34(6), 113-120. (in Chinese).

Wang, Y. Q., Wang, Z. X., Hu, X. G., Han, J. K., and Xing, H. J. (2016a). “Experimental study and parametric analysis on the stability behavior of 7A04 high-strength aluminum alloy angle columns under axial compression.” *Thin-Walled Struct.*, 108, 305-320.

Wang, Y. Q., Wang, Z. X., Yin, F. X., Yang, L., Shi, Y. J., and Yin, J. (2016b). “Experimental study and finite element analysis on the local buckling behavior of aluminium alloy beams under concentrated loads.” *Thin-Walled Struct.*, 105, 44-56.

Wang, Y. Q., and Wang, Z. X. (2016). “Experimental investigation and FE analysis on constitutive relationship of high strength aluminum alloy under cyclic loading.” *Adv. Mater. Sci. Eng.*, 2016.

Wang, Z. X., Wang, Y. Q., Zhang, J., Liu, M., and Ouyang, Y. W. (2018a). “Experimental investigation on deformation performance and stiffness of TEMCOR joints in aluminum alloy spatial reticulated shell structures.” *Proc., IASS Annual Symposia*, 23, 1-8.

Wang, Z. X., Wang, Y. Q., Sojeong, J., and Ouyang, Y. W. (2018b). “Experimental investigation and parametric analysis on overall buckling behavior of large-section aluminum alloy columns under axial compression.” *Thin-Walled Struct.*, 122, 585-596.

Wang, Z. X., Wang, Y. Q., Zhang, Y., Gardner, L., and Ouyang, Y. W. (2019). “Experimental investigation and design of extruded aluminium alloy T-stubs connected by swage-locking pins.” *Eng. Struct.*, 200, 109675.

Wang, Z. X., Wang, Y. Q., Yun, X., Gardner, L., and Hu, X. G. (2020). “Experimental and numerical study of fixed-ended high strength aluminum alloy angle section columns.” *J. Struct. Eng.*, http://doi.org/10.1061/(ASCE)ST.1943-541X.0002773.

Walport, F., Gardner, L., and Nethercot, D. A. (2019). “A method for the treatment of second order effects in plastically-designed steel frames.” *Eng. Struct.*, 200, 109516.

Yalçın, M. M., and Genel, K. (2019). “On the axial deformation characteristic of PVC foam-filled circular aluminium tube: Effect of radially-graded foam filling.” *Thin-Walled Struct.*, 144, 106335.

Yuan, H. X., Wang, Y. Q., Chang, T., Du, X. X., Bu, Y. D., and Shi, Y. J. (2015). “Local buckling and postbuckling strength of extruded aluminium alloy stub columns with slender I-sections.” *Thin-Walled Struct.*, 90, 140-149.

Yun, X., and Gardner, L. (2017). “Stress-strain curves for hot-rolled steels.” *J. Constr. Steel Res.*, 133, 36-46.

Zha, Y., and Moan, T. (2003). "Experimental and numerical prediction of collapse of flatbar stiffeners in aluminum panels." *J. Struct. Eng.*, 129(2), 160-168.

Zhao, Y., Zhai, X., and Wang, J. (2019). "Buckling behaviors and ultimate strengths of 6082-T6 aluminum alloy columns under eccentric compression–Part I: Experiments and finite element modeling." *Thin-Walled Struct.*, 143, 106207.

Zhou, F., and Young, B. (2009). "Concrete-filled aluminum circular hollow section column tests." *Thin-Walled Struct.*, 47(11), 1272-1280.

Zhou, F., and Young, B. (2018). "Concrete-filled double-skin aluminum circular hollow section stub columns." *Thin-Walled Struct.*, 133, 141-152.

Zhou, F., and Young, B. (2019). "Aluminium alloy channels subjected to web crippling." *Adv. Struct. Eng.*, 22(7), 1617-1630.

Zhu, P., Zhang, Q., Luo, X., Ouyang, Y., and Yin, J. (2020). "Experimental and numerical studies on ductile-fracture-controlled ultimate resistance of bars in aluminum alloy gusset joints under monotonic tensile loading." *Eng. Struct.*, 204, 109834.

Zhu, J. H., and Young, B. (2006). "Experimental investigation of aluminum alloy circular hollow section columns." *Eng. Struct.*, 28(2), 207-215.

Zhu, J. H., Li, Z. Q., Su, M. N., and Young, B. (2019). "Behaviour of aluminium alloy plain and lipped channel columns." *Thin-Walled Struct.*, 135, 306-316.

Zhu, S., Guo, X., Liu, X., and Jiang, S. (2018). "Bearing capacity of aluminum alloy members under eccentric compression at elevated temperatures." *Thin-Walled Struct.*, 127, 574-587.